



# Research on the Underground Water Inrush Mechanism Based on the Influence of Fault

Dongjie Zhang · Jianduo Wang · Shuai Guo · Jianli Cao

Received: 17 July 2021 / Accepted: 11 March 2022 / Published online: 1 April 2022  
© The Author(s), under exclusive licence to Springer Nature Switzerland AG 2022

**Abstract** In underground coal mining, the presence of high-permeability geological faults may cause a large amount of groundwater to suddenly erupt from the aquifer, resulting in undesirable casualties and economic losses. In order to deeply understand the mechanism of underground water inrush caused by typical faults in eastern China, the Zhuxianzhuang Coal Mine was selected as an engineering project case study. The study was analyzed by means of similar-physical experiments and numerical analysis. Research shows the following: (1) Similar-physical experiment results indicate that the evolution process of fault seepage can be divided into five stages: seepage initiation, seepage development, seepage mutation, seepage burst and seepage stability. Seepage

types can be summarized as initial pore flow, middle fracture flow, and late channel flow. It is clear that the water pressure, the thickness of aquifuge and the material gradation have an important influence on the seepage characteristics of fault. The migration and loss of particle fillings in fault are the main factors of seepage changes. Under the sustained action of water pressure, the permeability of fault continuously increases, and eventually the fracture flow converts into the channel flow, resulting in the formation of water inrush channels in fault. (2) Numerical simulation results indicate that the failure zone in the floor strata can be divided into mining-induced damage zone, effective water-resisting zone, and fault activation zone, the effective water-resisting zone is the key part of preventing water inrush. Cracks propagation, stress distribution and seepage evolution in the floor strata can be visualized during the formation of the water inrush pathway. Once mining-induced cracks intersect with cracks caused by fault activation, the seepage increases rapidly, and groundwater will flow into the mining face, resulting in water inrush. (3) When mining coal mines with high-permeability faults, the seepage in faults should be regularly monitored, and sufficient attention should be paid to the seepage mutation, which is crucial for accurately assessing the risk of water inrush from fault.

---

At the same time, the use of grouting and rock reinforcement methods can improve the integrity of the coal mine rock mass and play an important role in preventing water inrush hazards.

---

D. Zhang (✉) · S. Guo  
Institute of Mining and Coal, Inner Mongolia University of Science & Technology, Baotou 014010, China  
e-mail: 834381852@qq.com

J. Wang  
Petro China Liaohe Oilfield Company, Panjin 124010, China

J. Cao  
Center of Mining Research, School of Resources and Civil Engineering, Northeastern University, Shenyang 110819, China

**Keywords** Water inrush · Fault Seepage characteristics · Similar-physical experiments · Numerical simulation

## 1 Introduction

In China, many underground coal mines are threatened by groundwater (Lu et al. 2018; Yao et al. 2012; Zeng et al. 2017; Zuo et al. 2009). When the strength of the floor strata cannot withstand the high pressure of groundwater, the groundwater will break through the floor strata and rush into the mining face, causing serious casualties and economic losses (Zhang and Peng 2005). The three types of water hazards commonly encountered in coal mining in China include: (1) Water inrush from fractured aquifers in bedrock; (2) Water inrush from Cenozoic porous aquifers in alluvial plain; (3) Water inrush from Ordovician limestone aquifers (Jia 2012; Yin et al. 2015; Yang et al. 2004). The water inrush from Ordovician limestone aquifers has the most serious impact on the safe mining of the coal mine (Shi et al. 2017). The Ordovician limestone is a closed karst aquifer with high water pressure. Under the influence of the mining and inherent geological structures (such as collapse columns, faults and geological cracks), water inrush disasters are more likely to occur (Ma et al. 2004; Li et al. 2011; Liu et al. 2004). More than 130 coal mines in northeastern China have suffered water inrush disasters from the Ordovician limestone aquifer (Shi et al. 2017). The most serious water inrush event reached a maximum water inflow of 2065m<sup>3</sup>/min, resulting in the adjacent four mines were simultaneously submerged in a short time (Liu et al. 2017). Therefore, in the coal mining project, it is crucial to precisely know when, where, and how the groundwater inrushes can happen.

Research shows that rock is a heterogeneous material composed of various natural weakening points (Li et al. 2014), under the action of external forces (mining-induced and blasting vibration), the pre-existing weakening points inside the rock may open, close, spread, and form obvious fissures, these fissures constitute a high-permeability damage area, and create conditions for groundwater outburst (Yang et al. 2004; Liu et al. 2017). The development of the damage area is the result of the stress evolution under the influence of mining. When the stress concentration intensity at the abutment exceeds the strength that the rock itself can withstand, the floor strata will be destroyed and its permeability will increase rapidly, then potential water inrush disaster will occur. At the same time, it is worth noting that grouting and

rock reinforcement methods are used to improve the integrity of rock masses in coal mines (Chen and Li 2022; Chen and Liu et al. 2021; Chen and Zhao et al. 2021), which plays an important role in preventing water inrush hazards.

According to incomplete statistics, more than 80% of underground water inrush accidents in Chinese coal mines are related to faults (Wang et al. 2006; Zhang et al. 2014; Wu et al. 2004). As an important water inrush channel, faults are an important factor in the safe mining of underground coal mines. It has received extensive attentions in recent research. As shown in Fig. 1, when a fault exists in the near-mining area, the development of mining-induced damage zone in the floor strata is quite different from that without fault. Some studies have confirmed that the mechanical strength of the fault structure is lower than that of the intact rock mass under in-situ conditions (Islam and Shinjo 2009; Cao et al. 2001; Zhu and Wei 2011). When there is no fault (Fig. 1a), the possible water inrush route needs to pass through the complete floor, if the thickness and strength of the floor aquifuge are large enough, it is difficult for the occurrence of water inrush disaster; when a fault exists (Fig. 1b), the fault is gradually activating and the permeability is inevitably enhancing under the effect of the mining and high water pressure, which causes the groundwater to flow upward along the fault. At the same time, the existence of the fault causes the mining-induced damage area in the floor to expand toward the fault. The comprehensive effect greatly reduces the effective thickness of the aquifuge and the mechanical strength of the floor strata, and increases the risk of water inrush.

Although many scholars have studied the mechanism of groundwater inrush from theoretical analysis, in-situ geological measurements and numerical simulations (Yin et al. 2015; Lu and Wang 2015; Li et al. 2017; Liu et al. 2017), the evolution law of the seepage in fault and the failure analysis of the key position in the floor strata are not mentioned. In the mining process, when, where, and in what way of the development of water inrush remain unanswered, and the mining-induced cracks propagation, stress evolution, and the water inrush channel formation in the floor strata have not be elucidated. This is the key issue to be solved in this paper.

In this paper, an in-depth study was carried out in the Zhuxianzhuang Coal Mine (Eastern China) as

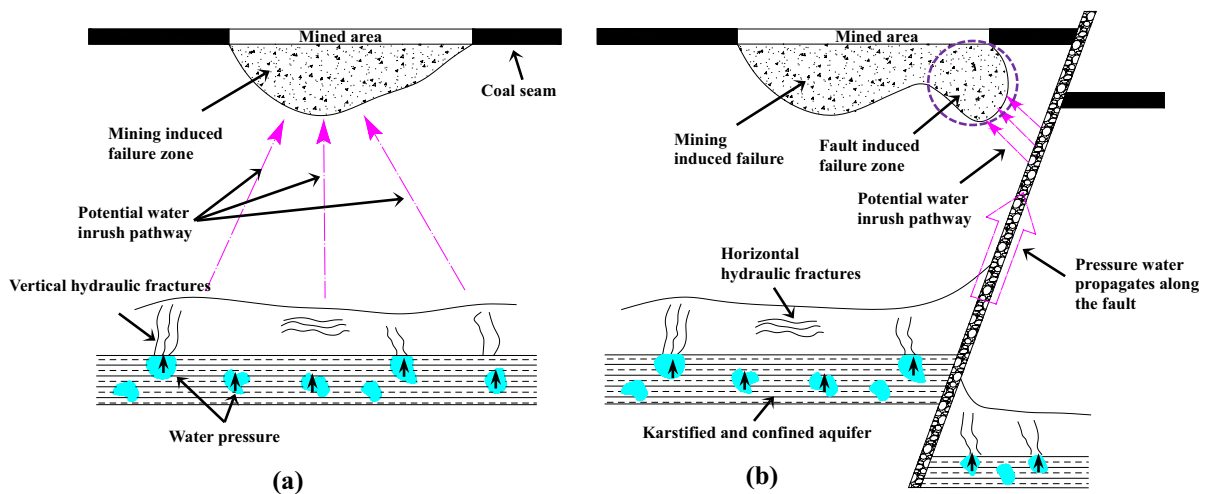


**Fig. 1** The schematic diagram of possible water inrush pathway with and without fault

an engineering case. A Similar-physical model for water inrush in fault was proposed. The evolution law of seepage in fault was studied, and the influence of water pressure, the thickness of the aquifer and the material gradation on the permeability characteristics of the fault was clearly expressed. Subsequently, combined with the coupled flow-stress-damage model (Yang et al. 2007; Tang et al. 2002; Zhang et al. 2009), a numerical software for rock failure process analysis (RFPA 2D) (Niu et al. 2017; Li et al. 2010) was used to study the water inrush mechanism in the Zhuxianzhuang Coal Mine. Important supplementary information that could not be directly observed on-site, such as when, where and how the water inrush may occur was captured. These are achieved by explicitly simulating the evolution pathway of underground water inrush caused by mining, so as to effectively reduce the risk of water inrush disasters in future mining.

## 2 Engineering Geology and Research Site

The Zhuxianzhuang Coal Mine is a gently inclined thin seam and is located in Suzhou City, Anhui Province, Eastern China (Fig. 2). The geographical coordinates are 33°36'N latitude and 117°05'E longitude, the mine area is about 26.3 square kilometers. The surface elevation is between +110 and +130 m. This area is a temperate continental monsoon climate with

an average annual rainfall of about 690 mm, and an annual production of about 25 million tons. The geological exploration was completed by the Geological Exploration Bureau of Anhui province in 2010.

According to the exploration results, the rock stratum is mainly composed of the Quaternary, Permian, Carboniferous and Ordovician systems. The rock mass near the coal seam is mainly composed of sandstone, mudstone, coal seam and Ordovician limestone (Fig. 3). The F13 fault with an inclination of 55° and the thickness of 4~8 m cut the intact rock formation and forms a fault fracture zone. The coal mining occurred in the 8# coal seam located in the Carboniferous strata. According to the on-site measurement results, the Ordovician limestone is located 40 m below the coal seam with an in-situ water flow of 0.5~0.9 L/(s.m) and an average water pressure of 3.8 MPa, which is the main aquifer that causes the groundwater inrush. Comprehensive rock strata column diagram is shown in Fig. 4.

The mining face No.866 was the main production area (Fig. 5), and a typical water inrush accident occurred during the mining on January 30, 2015. When the mining advances to a distance of 60 m from the fault (F13), the water inflow of roadway floor quickly increased from the previous 30m<sup>3</sup>/h to 235m<sup>3</sup>/h, and a salient appeared in roadway floor. Unfortunately, this phenomenon did not attract the attention of the operators. When the distance reduced to 45 m, groundwater suddenly

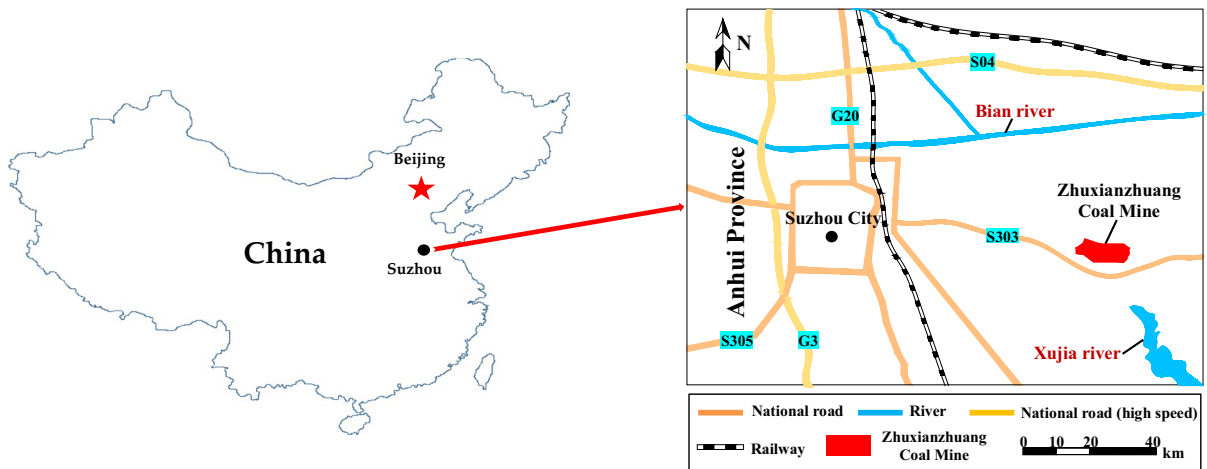
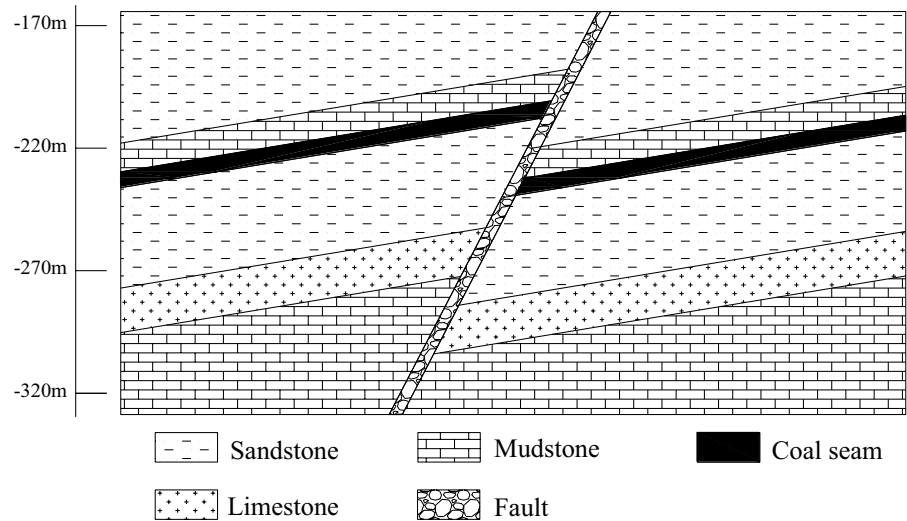


**Fig. 2** Location of Zhuxianzhuang Coal Mine in Anhui Province, Eastern China

**Fig. 3** Vertical section of the mining face in the Zhuxianzhuang Mine



flowed into the mining face and the mining face was inundated in a few hours, resulted in 34 workers being trapped in underground. According to the hydrogeological survey results, this serious water inrush accident would be caused by high-pressure water passing through the fault to penetrate the floor strata. In order to elucidate the mechanism of water inrush from the mining face No.866, the similar-physical experiments and numerical analysis of the water inrush were carried out.

### 3 Similar-physical Experiment

#### 3.1 Experimental Model and Program Design

This chapter will focus on the seepage characteristics of groundwater along the fault. According to the composition and distribution of the in-situ fault near the mining face No.866, the Similar-physical model of water inrush in fault was designed according to the geometric similarity scale. As shown in Fig. 6.

serial number	column diagram	thickness/m	lithology
1		25.2~33.7	sandstone
2		8.7~12.5	mudstone
3		4.6~6.2	8# coal seam
4		38.5~46.1	sandstone
5		16.3~22.4	limestone
6		25.5~32.2	mudstone

**Fig. 4** Comprehensive rock strata column diagram

The system was mainly composed of three parts: water tank, pump and similar model. The size of the similar model was 300×300×800 mm, and the model was set from bottom to top as flume, confined aquifers, aquifuge and fault, surrounding rock and the apical plate are constructed of wood and impervious cement mortar. The ratio of the water–cement and cement–sand was 0.3 and 0.4, respectively. The average uniaxial compressive strength was about 37.5 Mpa. According to the in-situ geological investigation and laboratory testing, the fault is mainly composed of fractured rock and particle fillings with the ratio of 1:1.5. In order to

approximate the on-site fault condition, for the simulated fault material, limestone with a particle size of 15~25 mm was selected as aggregate, and sandstone with a particle size of 1~5 mm was selected as fillings. This is the most important part of simulating water inrush from fault above the confined aquifer. In this study, water flow and particle fillings mass for analysis were obtained from the top outlet of the model. The experimental scheme is shown in Table 1.

### 3.2 Experimental Data Analysis

The seepage parameters needed to be obtained in the experiment mainly include the water inflow ratio, the particle fillings inflow ratio, the porosity and the permeability. The water inflow ratio (ml/s) is obtained by the following formula:

$$F' = \frac{\Delta F}{\Delta t} \tag{1}$$

where  $\Delta F$  is the water inflow in different periods, and  $\Delta t$  is the time of water inflow which is generally 10 s in the experiment. The expression of particle fillings inflow ratio (g/s) is as follows:

$$Q' = \frac{\Delta M}{\Delta t} \tag{2}$$

where  $\Delta M$  is the mass of particle fillings collected in the experiment. Fault porosity is calculated by the following formula:

**Fig. 5** Plan view of mining face No. 866 in the Zhuxi-anzhuang coal mine

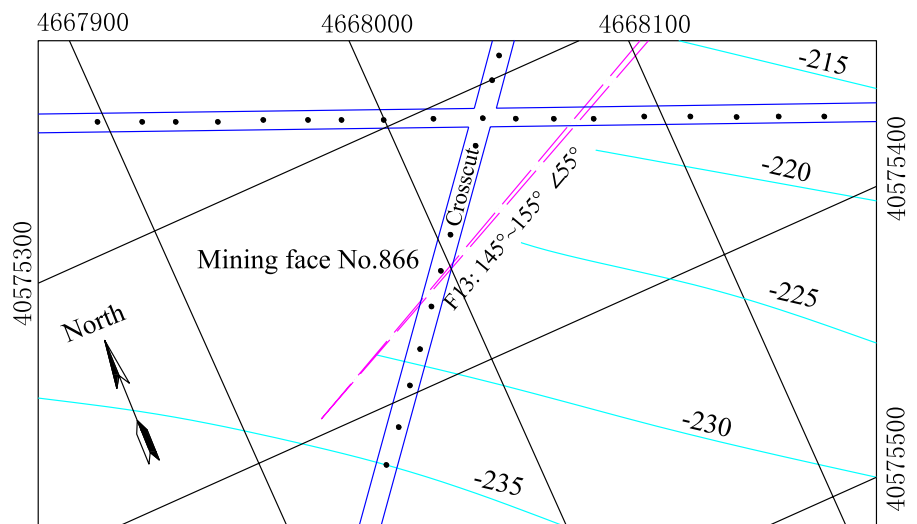


**Fig. 6** Physical model of water inrush from fault

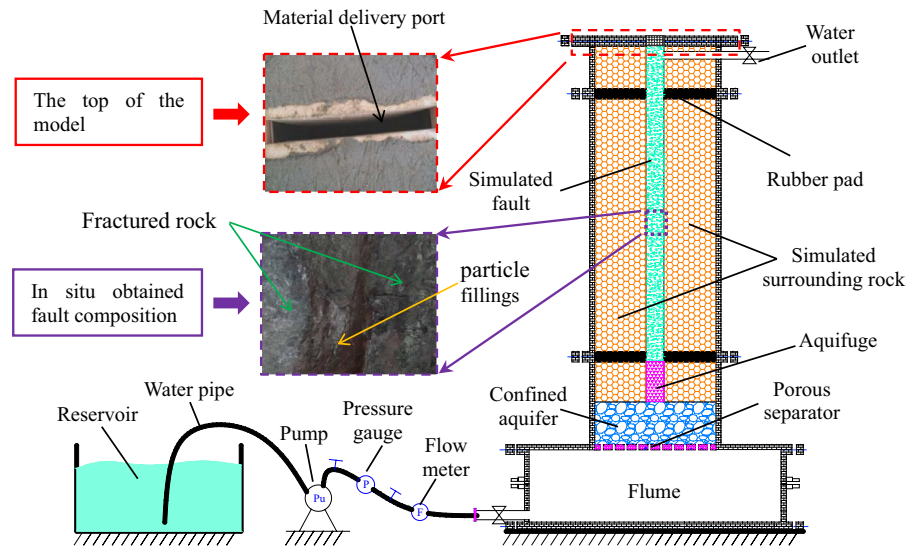


**Table 1** The main experimental scheme

Program	Major influencing factor	Value	Other conditions
1	Water pressure in aquifer $P$ / MPa	0.3	Material gradation in fault (fractured rock to particle fillings) $R = 1:1$ ; Thickness of aquifuge $T = 40$ mm
2		0.5	
3		0.7	
4	Material gradation in fault (fractured rock to particle fillings) $R$	1:1	Water pressure in aquifer $P = 0.5$ MPa; Thickness of aquifuge $T = 40$ mm
5		1:3	
6		1:5	
7	Thickness of aquifuge $T$ / mm	40	Material gradation in fault (fractured rock to particle fillings) $R = 1:1$ ; Water pressure in aquifer $P = 0.5$ MPa
8		60	
9		80	

$$I' = \frac{\Delta M}{\rho \cdot V} \tag{3}$$

where  $V = l \cdot d \cdot h$ , and  $l$  is the length of the fault,  $d$  is the width of the fault,  $h$  is the effective seepage height of the fault, the increase in fault porosity in different periods is as follows (Kong 2010):

$$\Delta I' = I'_0 + \frac{1}{\rho \cdot V} (\Delta M_1 + \Delta M_2 + \dots + \Delta M_n) \tag{4}$$

where  $I'_0$  is the initial porosity. The fault seepage velocity is expressed as follows:

$$v = \frac{\eta}{\mu} \cdot \frac{\partial P}{\partial c} = \frac{\Delta F}{l \cdot d} \tag{5}$$

where  $\eta$  is the permeability,  $\mu$  is the dynamic viscosity of the water, and  $P$  is the water pressure. Assuming that the seepage process of the pressure water along fault conforms to Darcy's law, there is:

$$\frac{\partial P}{\partial c} = \frac{P}{h} \tag{6}$$

Then, the expression of the fault permeability is determined as follows.

$$\eta = \frac{\mu \cdot P \cdot \Delta F}{l \cdot d \cdot h} = \frac{\mu \cdot P \cdot \Delta F}{V} \tag{7}$$

### 3.3 The Seepage Evolution Process in Fault

According to the experimental parameters provided in the scheme 1, similar experimental results show that the process of the water inflow can divide into five stages (Fig. 7a). “①” represents the initial stable stage, “②” represents the early slowly increase stage, “③” represents the suddenly decrease stage, “④” represents the middle rapid increase stage, “⑤” represents the late smooth fluctuation stage.

By observing the permeability curve, the seepage process can also be divided into five stages (Fig. 7d). "A" represents the seepage initiation stage, "B" represents the seepage development stage, and "C" represents the seepage mutation stage. "D" represents the seepage outburst stage, and "E" represents the seepage stable stage. In the first stage, due to the presence of the aquifuge, the high-pressure water did not completely penetrate into the fault, so the water inflow ratio, the permeability and the particle fillings inflow ratio were kept constant, and the values were basically zero. In the second stage, the water inflow ratio in fault increased slowly, indicating that the high-pressure water has passed through the aquifuge and entered the fault. Under the influence of water pressure, the fault is initially activated, part of the particle fillings flow out from the outlet, and the permeability increases. In the third stage, the water

represents the seepage mutation stage. "D" represents the seepage outburst stage, and "E" represents the seepage stable stage. In the first stage, due to the presence of the aquifuge, the high-pressure water did not completely penetrate into the fault, so the water inflow ratio, the permeability and the particle fillings inflow ratio were kept constant, and the values were basically zero. In the second stage, the water inflow ratio in fault increased slowly, indicating that the high-pressure water has passed through the aquifuge and entered the fault. Under the influence of water pressure, the fault is initially activated, part of the particle fillings flow out from the outlet, and the permeability increases. In the third stage, the water

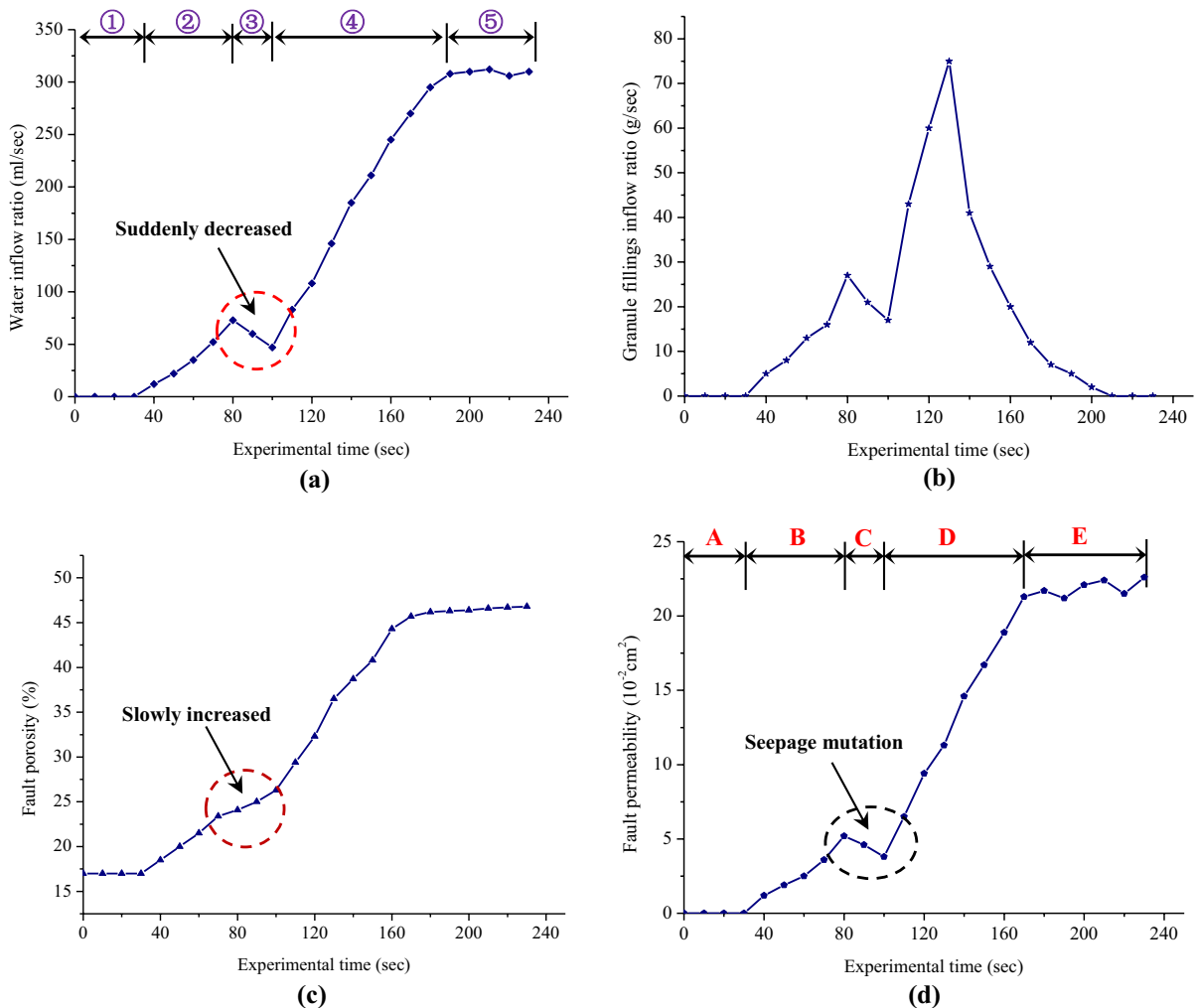


**Fig. 7** Variation characteristics of seepage parameters obtained by experiments: **a** water inflow ratio; **b** particle fillings inflow ratio; **c** fault porosity; **d** fault permeability



inflow and permeability decreased in a short time, the reason was that particle fillings are consolidated during the migration, and the formed seepage holes were partially blocked. In the fourth stage, the water inflow and permeability increased rapidly, indicating that under the continuous action of pressurized water, the blocked parts were washed away, resulting in a rapid increase of fault porosity (Fig. 7c), with the migration of large amounts of particle fillings, a water inrush channel gradually formed. In the fifth stage, the water inflow in fault kept stable, the particle fillings inflow ratio decreased rapidly and approached zero (Fig. 7b), and the porosity and permeability were close to constant, indicating the water inrush channel was completely formed at this time.

### 3.4 Analysis of the Influence Factors of Seepage

#### 3.4.1 Water Pressure

For the selection of water pressure in the experiment, it is mainly obtained based on field measurement. The distribution range of water pressure measured at different water seepage positions in the working face is about 0.3~0.7 MPa. For this reason, in physical experiments, in order to clarify the influence of different water pressure distribution conditions on fault penetration, the water pressure is determined to be 0.3 MPa, 0.5 MPa and 0.7 MPa. The variation of seepage under different water pressures is shown in Fig. 7. When the water pressure was 0.3 MPa, the inflow ratios of the water and particle fillings, the initial growth rate of porosity and permeability were relatively small. With the increasing of water pressure, the barrier effect of the aquifuge reduced, resulting in faster seepage, the water inflow ratio and permeability were also greatly accelerated, and the stable seepage stage was achieved earlier (when the water pressures were 0.3, 0.5 and 0.7 MPa and the times for stable seepage were 190 s, 180 s and 160 s, respectively) (Fig. 8a). As shown in Fig. 8b, as the water pressure increased, the peak of the particle fillings inflow ratio also increased significantly. The larger water pressure took away more particle fillings and the time to reach the peak was also advanced. After the peak, there was no significant difference in the decrease rate of the fillings inflow ratio. It can be concluded from Fig. 8d that the higher water pressure can make the permeability reach the peak quickly. It is worth noting

that the consolidation of particle fillings is more pronounced at low water pressure, which may disappear as the water pressure increases. Therefore, it can be concluded that water pressure is an important factor in the evolution of seepage channels in fault. The ability of the water to erode the particle fillings will be inevitably raised with water pressure increasing, resulting in more particle fillings being carried away at a faster rate.

#### 3.4.2 The Thickness of Aquifuge

The variation of seepage under different thicknesses of aquifuge is shown in Fig. 9. With the change of the thickness, the delayed growth of the water and fillings inflow ratio and the permeability was obvious (Fig. 9a and d), indicating that the thicker aquifuge increased the time that the water flowed through the aquifuge, and it had less effect on the consolidation during the migration of the particle fillings, but only changed the time of the occurrence of the seepage mutation. As the thickness of the aquifuge increased, the maximum value of the fillings inflow ratio decreased gradually, and the time for the peak was delayed (when the thickness of aquifuge were 40, 60 and 80 mm and the times for the peak were 130, 140 and 150 s, respectively) (Fig. 9b), and the time to form a stable water inrush channel had increased. As the greater thickness of the aquifuge, the greater barrier of water flow through the aquifuge, which caused the migration mass and migration speed of particle fillings were restricted under the water erosion (Fig. 9d). Figure 8c showed the curves of porosity-time for different aquifuge thicknesses, the initial porosity increased gradually under the influence of water pressure within 0~80 s. After 80 s, the porosity increased rapidly. It is worth noting that the greater thickness of the aquifuge is, the smaller growth of the fault porosity and the later stable seepage is.

#### 3.4.3 Material Gradation in Fault

As shown in Fig. 10, as the ratios of fractured rock to particle fillings increased, the water inflow ratio and the fault permeability increased gradually, with the smallest increasing relative to the water pressure and the thickness of aquifuge. For the seepage change process, when the ratios of fractured rock to particle fillings were 1:3, 1:5 and 1:7, the times to



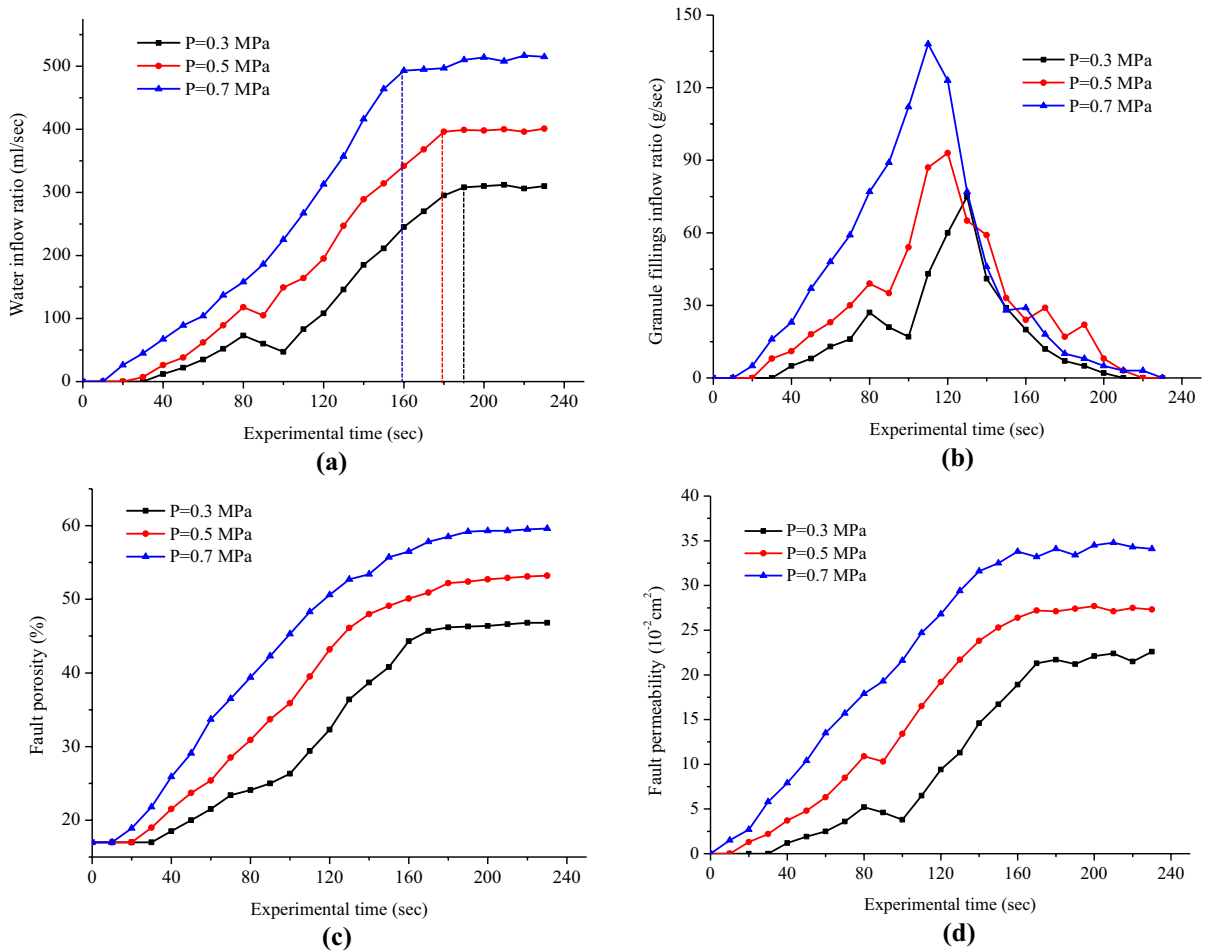


**Fig. 8** Variation characteristics of seepage parameters under different water pressures

reach stable seepage were 190, 170 and 150 s, respectively (Fig. 10d), the proportion of higher particle fillings increased the time that the seepage reached a stable period. At the same time, the particle fillings inflow ratio increased, and the time to reach the peak advanced gradually (Fig. 10b). As a result, the porosity in fault changed greatly, and a significant porosity inflection point appeared (Fig. 10c). This phenomenon can be explained as follows: the higher proportion of the particle fillings is, the higher degree to which the particle fillings may be washed and migrated. Subsequently, the sustained action of the water pressure removes more particle fillings in a short time, and the migration of more particle fillings leads to greater porosity changes. It is worth noting that with the increase of particle fillings, the seepage mutation stage is gradually weakened. It can be

speculated that this stage will disappear as the proportion of particle fillings continues to increase. It is because the increase of the particle fillings results in a larger potential pore between the fractured rocks, and the rapidly increasing porosity reduces the probability of consolidation of the fillings during the migration process.

### 3.4.4 The Seepage Evolution Mechanism

According to the experimental results that were described above, the research indicate that the particle fillings in fault is not eroded due to the presence of the aquifuge in the initial stage, and the seepage parameters are basically unchanged. Under the influence of continuous high-pressure water, the aquifuge is gradually damaged, the particle fillings in fault are

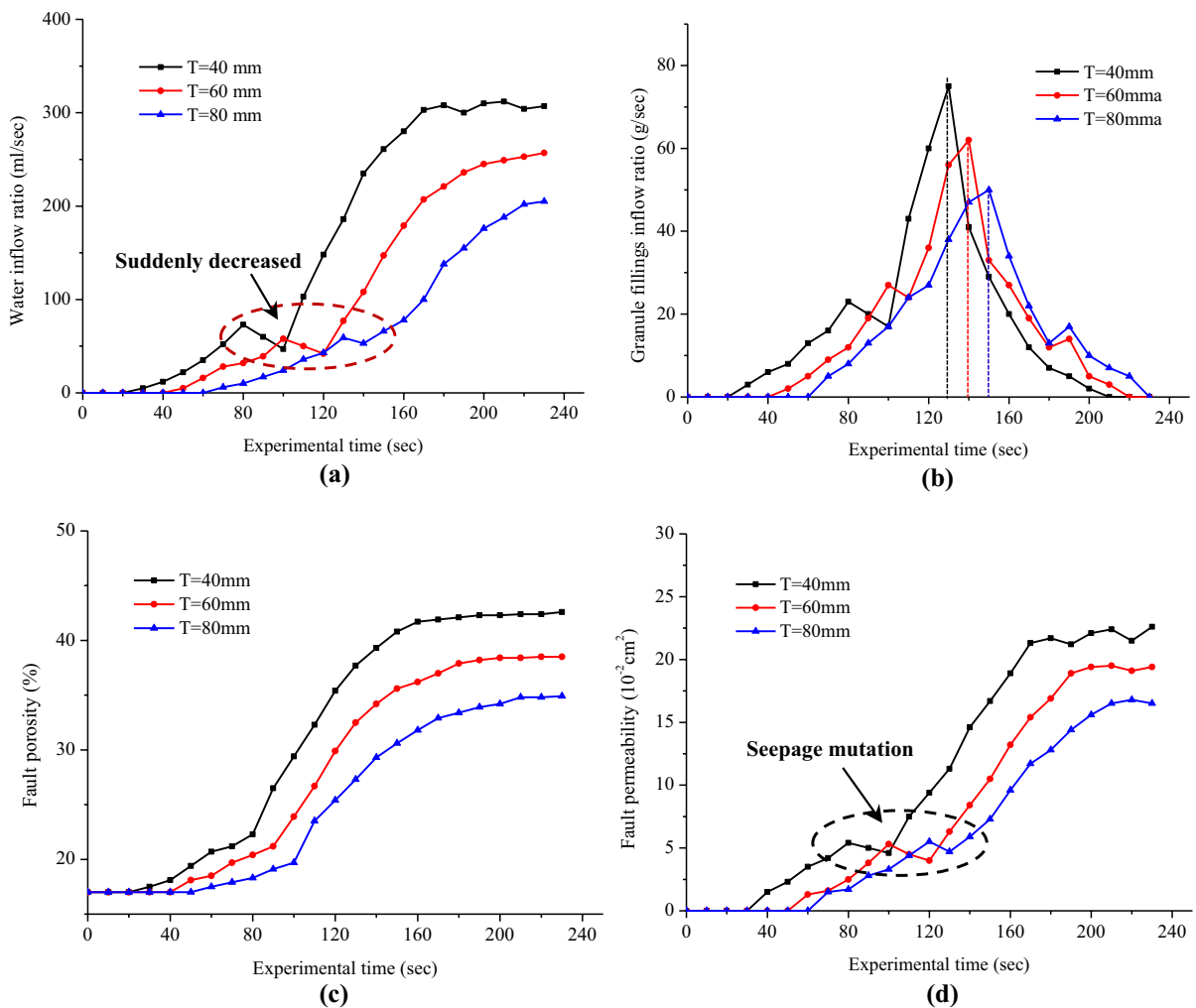


**Fig. 9** Variation characteristics of seepage parameters under different thickness of aquifuge

eroded and slowly migrated, and gradually flows out from the water outlet, causing the changes of porosity and permeability, the seepage at this time is mainly pore flow. The particle fillings will be continuously washed and flowed out, if the water inflow ratio and/or permeability suddenly decrease, it indicates that the seepage will mutate, and the seepage will convert into fracture flow after the mutation, resulting in a rapid increase of water inflow ratio, porosity and permeability. In addition, the increase of porosity and permeability will bring greater permeability, resulting in rapid migration of large amounts of particle fillings under water erosion. The porosity and permeability in fault then continue to increase until it remains substantially stable, the seepage is converted

from fracture flow to channel flow, and the water inrush channel is formed. The seepage process can be divided into three types, pore flow, fracture flow and channel flow. During the process of pore flow to fracture flow conversion, special attention should be paid to the seepage mutation stage, it is crucial for the accurate assessment of water inrush risk. In addition, for different water pressures, the thickness of the aquifuge and the material gradation show a significant difference. It is indicated that the seepage characteristics in fault are affected not only with time but also with different geological structural conditions.

The in-situ stress is a natural stress before the occurrence of mining activity. Compared with rock excavation, it can be seen as a constant stress field (Zhao et al.

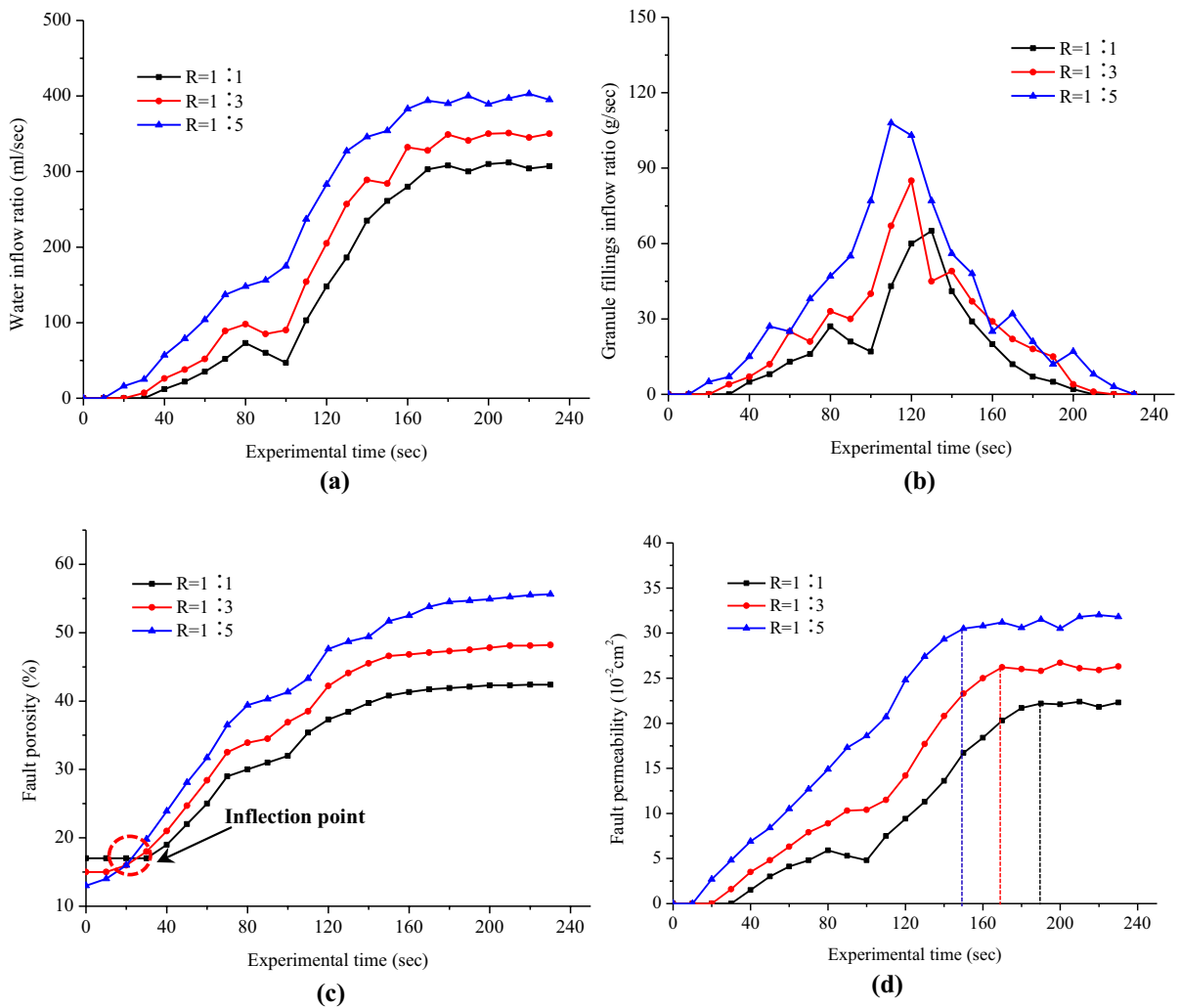


**Fig. 10** Variation characteristics of seepage parameters under different material combinations

2007). When the coal seam is mined, the stress balance will be destroyed. Under the influence of water pressure, the generated fissures create conditions for groundwater to pass through the fault. At the same time, the particle fillings in fault are continuously washed and migrated under the high water pressure, resulting in the type of seepage gradually changing from the pore flow and the fracture flow to the channel flow. Eventually, the high-pressure groundwater passes through the fault and continuously impacts the aquifuge between the fault and floor strata, once the aquifuge is damaged, a potential pathway for groundwater inrush is formed. It can be considered that the mining fissures, the high pressure aquifer and the migration of the particle fillings are the

main factors for the formation of the water inrush channel in fault. Therefore, the groundwater inrush affected by faults has a complex nonlinear relationship and is a typical fluid–solid coupling problem. In order to further explain the water inrush mechanism of the mining face No.866 in the Zhuxianzhuang Coal Mine, the numerical simulation will be used for analysis.

#### 4 A Case Study Based on Numerical Simulation from Zhuxianzhuang Coal Mine

##### 4.1 Principles of Numerical Methods

In this study, the rock failure process analysis (RFPA 2D) code is used to simulate the water inrush in the Zhangxianzhuang Coal Mine. This code introduced the homogeneity of the rock material properties, and was originally developed by Dalian Mechanics Software Co. Ltd. in China (RFPA User Manual 2005). RFPA 2D can simulate nonlinear deformation of a quasi-brittle rock with an ideal elastic-brittle constitutive law for local material (Tang 1997). The software can more intuitively display the seepage development and the process of rock formation failure. It can clearly determine the temporal and spatial relationship of water inrush, and has obvious advantages in the study of water inrush mechanism in mines. On account of the heterogeneity of rock-like materials, the local mechanical parameters of the elements are assumed to follow Weibull's distribution, which is defined as follows (Fang and Harrison 2002; Ma et al. 2011; Weibull 1951):

$$\varphi(c, m) = \frac{m}{c_0} \left( \frac{c}{c_0} \right)^{m-1} \exp \left[ - \left( \frac{c}{c_0} \right)^m \right] \quad (8)$$

where  $c$  is the parameter of the element (Young's modulus, Poisson's ratio or strength),  $c_0$  is the average of the element parameter,  $m$  is a homogeneity index, which can be defined by the shape of the distribution function. A larger  $m$  is a more homogeneous material. This numerical method, based on discontinuum mechanics, seepage hydraulics, and damage mechanics, can be used to perform stress analysis, seepage analysis, failure analysis, and fluid-stress-damage (FSD) coupling analysis.

The basic assumptions of this numerical method are: (1) the rock is fully saturated; (2) The flow of the groundwater conforms to the Biot consolidation theory; (3) The change of permeability is determined by the state of stress during the elastic deformation phase, and the permeability is significantly increased when the elements are damaged (Yang et al. 2004). The mechanical and flow equations based on stabilizing behavior are expressed as follows:

Balance equation:

$$\frac{\partial \sigma_{ij}}{\partial x_{ij}} + Y_j = 0 \quad (i, j = 1, 2, 3) \quad (9)$$

where  $\sigma_{ij}$  is the total stress in the  $ij$ -plane and  $Y_j$  is the body force in the  $j$ th direction.

Geometrical equation:

$$\varepsilon_{ij} = \frac{1}{2} (\tau_{i,j} + \tau_{j,i}) \quad \varepsilon_v = \varepsilon_{11} + \varepsilon_{22} + \varepsilon_{33} \quad (10)$$

where  $\varepsilon_{ij}$  is the strain and  $\tau_i$  is the displacement in the  $i$ th direction.

Constitutive equation:

$$\sigma'_{ij} = \sigma_{ij} - \psi p \delta_{ij} = \vartheta \delta_{ij} \varepsilon_v + 2G \varepsilon_{ij} \quad (11)$$

where  $\sigma'_{ij}$  is the effective stress in the  $ij$ -plane,  $p$  is the pore pressure,  $\psi$  is the coefficient of pore-fluid pressure,  $\vartheta$  is the Lamé coefficient,  $G$  is the shear modulus, and  $\delta_{ij}$  is the Kronecker constant.

Seepage equation:

$$k \nabla^2 p = \frac{1}{\ell} \frac{\partial p}{\partial t} - \psi \frac{\partial \varepsilon_v}{\partial t} \quad (12)$$

where  $k$  is the coefficient of permeability,  $\ell$  is the Biot constant.

Coupling equation:

$$k(\sigma, p) = \xi k_i \exp [-\beta(\sigma_{ii}/3 - \psi p)] \quad (13)$$

where  $k_i$  is the initial coefficient of permeability,  $\xi$  and  $\beta$  are material constants.

In the elastic damage stage, the permeability of rock materials will inevitably increase with the generation, propagation and agglomeration of cracks. The internal reason for the rapid increase in rock permeability is that the seepage channels are formed by the passage of a large number of microcracks (Yuan and Harrison 2005; Souley et al. 2001; Minkoff et al. 2003). When using RFPA 2D for simulation, the permeability coefficient of the damaged rock is expressed as:

$$k_e = \frac{b^2 \rho_n g}{12 \mu_n} = \frac{\sqrt[3]{V^2 \rho_n g}}{108 \mu_n} \varepsilon_v^2 \quad (14)$$

where  $V$  is the change of volume of the element,  $\mu_n$  is the viscosity coefficient of the fluid, and  $g$  is the acceleration of gravity.

When performing numerical experiments, the model is loaded in a quasi-static manner. During each loading process, the seepage and stress equations are solved and coupled analysis is performed. The stress field is then automatically checked, and the stiffness and strength of the elements in the model that exceed the given threshold are reduced, and the permeability is increased. The next load increment is added only when there are no more elements strained beyond the strength-threshold corresponding to the equilibrium stress and compatible strain field. Throughout the simulation, the main state variables (stress, displacement) and material properties (elastic modulus, permeability) are nested in the initial heterogeneous field, and the damage development and water inrush process of the rock mass are tracked in an intuitive way.

### 4.2 Numerical Modeling

In this study, based on the specific geological and geometric conditions, the geological profile of the mining face (No. 866) is selected and modeled for the numerical simulation. The numerical model is shown in Fig. 11, the analysis domain is

300×240 m, and the model is divided into a mesh with 450×360=162,000 elements. A compressive vertical stress ( $\sigma_v$ ) of 4.0 MPa is imposed on the top boundary to represent the stress induced by the overburden strata. A water pressure of 3.8 MPa is applied to the external boundary of the Ordovician limestone, and used to simulate confined aquifers.

Normal displacements are constrained on the right, left and bottom boundaries; the model is affected by its own gravity. The draw is simulated by gradually removing the coal seam with a depth ranging of -220 m bsl, and for each step, the excavation size is 5 m in height and 10 m in length. The model is calculated in a quasi-static manner to achieve a balanced state, and the calculation process is assumed to be a plane strain problem. The mechanical parameters of the rock mass are mainly obtained through laboratory tests (Mohamma et al. 1997; Nicholson et al. 1990), and calibrated in accordance with the RMR classification system (Bieniawaki et al. 1973, 1987). Rock mechanical parameters are obtained through experiments, as shown in Table 2. In the mine design, a 40 m long coal pillar was used as a safety pillar to prevent water inrush from the fault.

**Fig. 11** Numerical model for groundwater inrush in Zhuxianzhuang coal mine

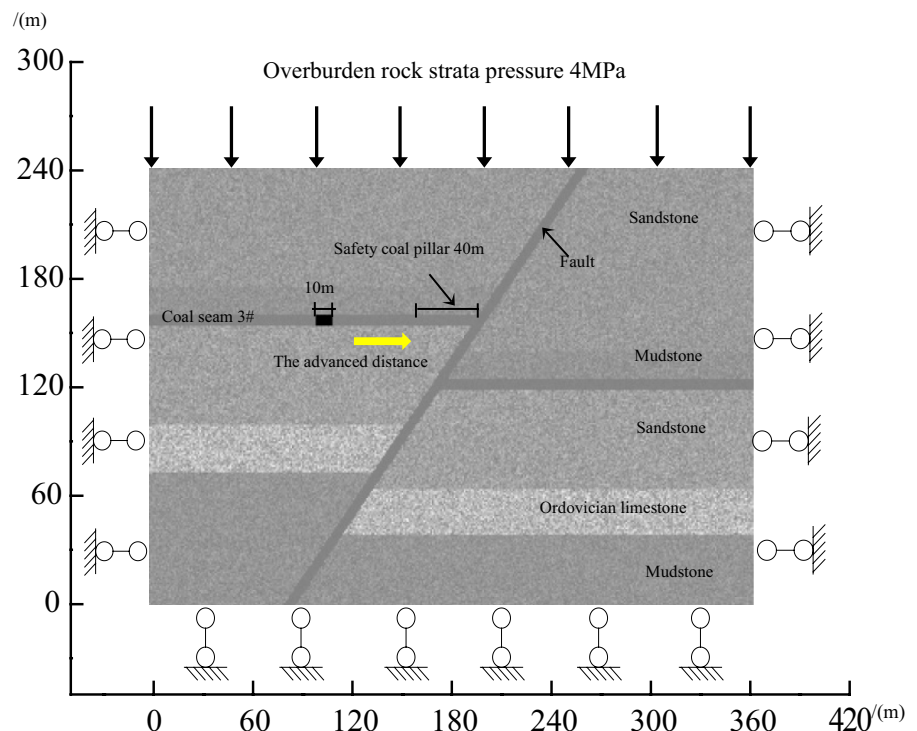


**Table 2** Rock mass mechanics parameters used in the simulations

Rock type	Young's modulus $E_0$ (GPa)	Compressive strength $f_c$ (MPa)	Tensile strength $f_t$ (MPa)	Internal cohesive angle $\varphi$ (deg)	Poisson's ratio $\nu$	Weight $\rho$ (kg/m <sup>3</sup> )	Hydraulic conductivity $\tau$ (m/d)	Pore water pressure coefficient $\alpha$
Sandstone	3.2	7	0.35	38	0.22	2500	0.15	0.1
Mudstone	2.7	4.2	0.21	30	0.27	2350	0.15	0.1
Coal seam	1.8	2.4	0.12	30	0.30	2100	0.1	0.05
Ordovician limestone	6.5	8.4	0.42	33	0.25	2650	86.5	0.95
Fault	1.2	2.0	0.1	28	0.35	2200	80.5	0.95

### 4.3 Numerical Results

Figure 12 and Fig. 13 show the stress field evolution process and the maximum principal stress distribution in the seam floor, respectively. The gray scale in the model indicates the relative size of the shear stress of the elements, the brighter the gray scale, the larger the shear stress. The black elements indicate the damage unit, and the crack is formed by the connection of a large number of damage units.

The numerical simulation results show that when the advancing distance of the 8# coal seam reaches 20 m, the stress concentration mainly appears on both sides of the opening (Fig. 12a), the seam floor is slightly damaged, and the maximum compressive stress of the right coal rib is 5.15 MPa (Fig. 13). When the advancing distance reaches 30 m, the stress is released at the middle of the seam floor where the maximum compressive stress is 2.28 MPa, and the stress concentration area extends downwards about 2 times the mining height along the right coal rib (Fig. 12b). When the advancing distance reaches 40 m, the stress concentration of the aquifuge between the fault and the seam floor is more serious (Fig. 12c), and the maximum compressive stress is 5.28 MPa. The continuous influence of water pressure and mining-induced stress further reduces the effective thickness of the aquifuge, and the potential water inrush channel will appear between the seam floor and fault (Fig. 12d), the maximum compressive stress of the right coal rib is 4.63 MPa. Once the water inrush channel is completely formed (Fig. 12e), the stress concentration develops upward along the fault, and the stress shadow area appears near the water inrush channel, and the maximum compressive stress of the right coal rib decreases to 4.12 MPa. It

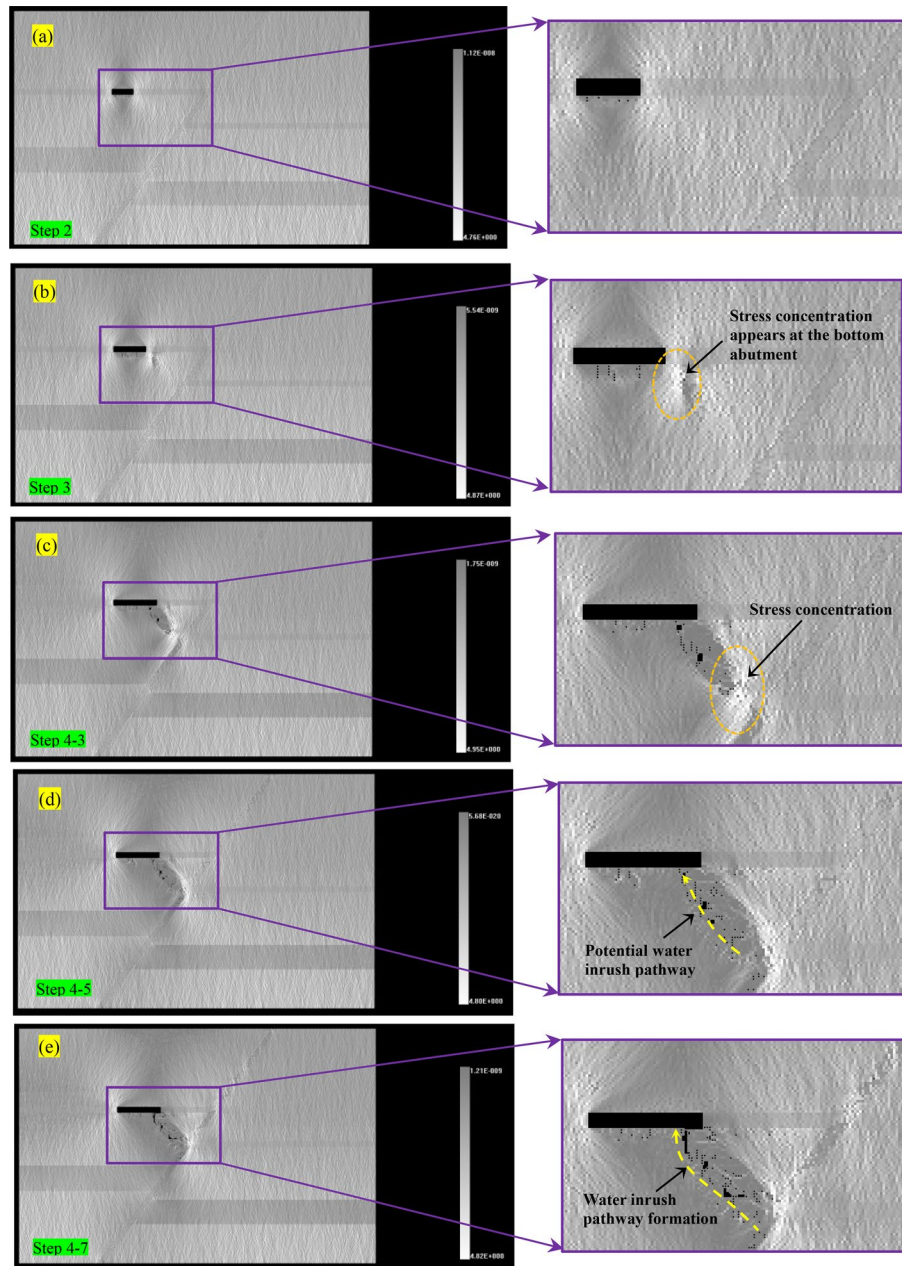
is worth noting that during the whole mining process, the stress of the excavation floor is continuously redistributed, and the maximum compressive stress of the left coal rib is gradually increased, and the maximum compressive stress of the right coal rib firstly increased and then gradually decreased (Fig. 13). The stress evolution characteristics before and after the formation of the water inrush channel are further clarified. In practice, since weak structures such as pores and micro-cracks are distributed in the rock mass, the stratum and fault are heterogeneous, and resulting in the inter-penetration and development of the cracks in an irregular manner. Therefore, the water inrush pathway is flexural. When mining coal mines with faults and high-pressure aquifers, if the stress of the coal rib firstly increases and then decreases, we should pay special attention to prevent the occurrence of water inrush disasters.

Figure 14 and Fig. 15 show the damage development process and the vertical displacement in the seam floor, respectively. The red points in the model represent tensile damage, the white points represent shear damage, and the black points represent accumulative damage.

In the initial stage of mining, the tensile damage mainly occurred in the seam floor. The maximum vertical displacement of the seam floor reached 6.6 mm, and the effective aquifuge remained basically intact. At this time, the fault was initially activated by the influence of the high water pressure, and the floor strata could be divided into three influenced zone, mining-induced damage zone, effective water-resisting zone, and fault activation zone (Fig. 14a). As the mining progresses, the tensile damage continued to develop along the seam floor, and a small amount of shear failures occurred in the effective water-resisting



**Fig. 12** The critical pathway for water inrush by the evolution of stress field



zone (Fig. 14b). At this time, the fault is further activated, and the maximum vertical displacement of the seam floor reached 11.9 mm. When the mining distance reached 40 m, due to the existence of fault, the development of the damage zone in the right floor was significantly higher than that in the left floor, the activation of the fault was intensified, and the effective thickness of the aquifuge was reduced from the initial 60 m to 28 m. Since the cracks generated by

the fault activation and the mining did not penetrate, the aquifuge in the effective water-resisting zone remained basically stable (Fig. 14c), although the maximum vertical displacement of the seam floor reached 48.7 mm (Fig. 15). As the strength of the aquifuge decreased, the tensile damage continued to extend to the fault, the effective thickness of the aquifuge was reduced to 13 m (Fig. 14d), and the maximum vertical displacement of the seam floor reached



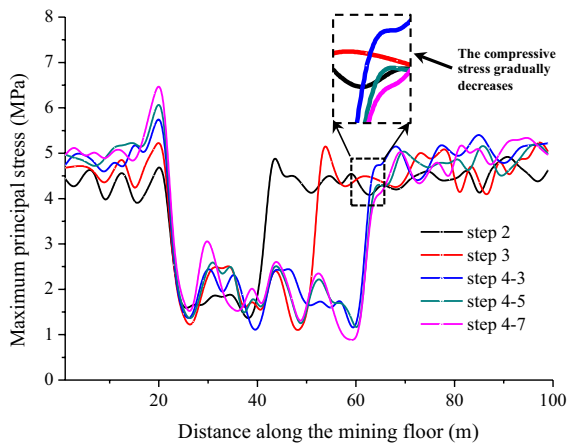


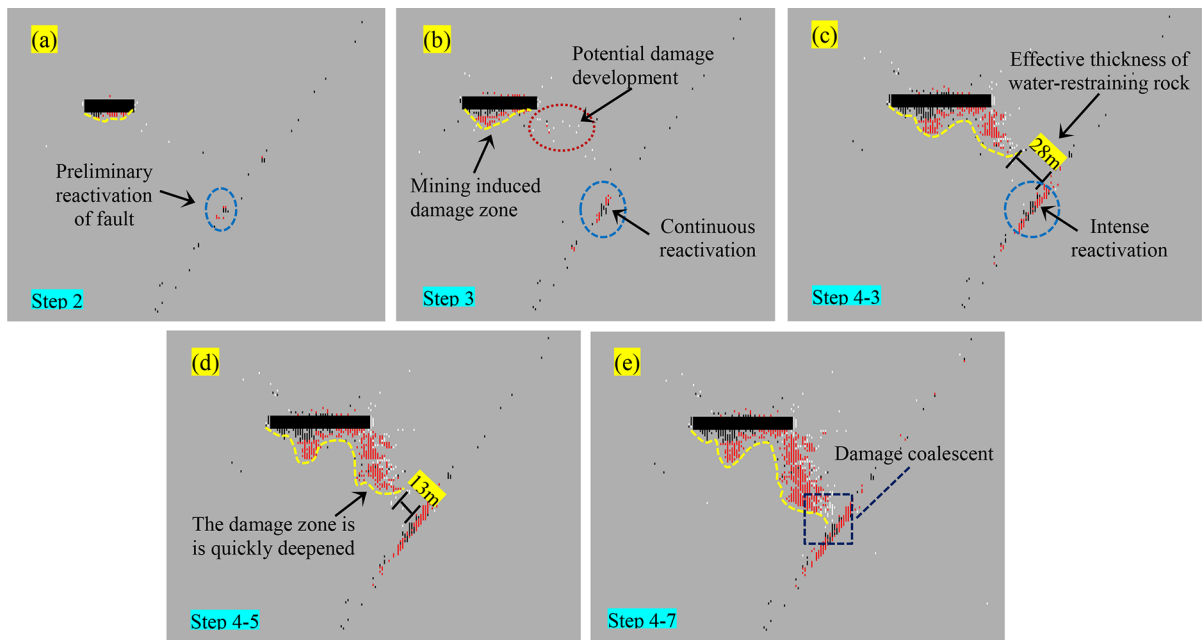
**Fig. 13** The distribution of maximum principal stress in the mine floor

147.6 mm (Fig. 15), indicating that a potential water inrush channel was being bred. Under the influence of the water pressure and mining, a large amount of shear failures occurred in the residual aquifuge, and continued to expand to the fault activation zone. Finally, the mining-induced damage zone was connected to the fault activation zone, the water inrush channel was formed with the effective water-resisting

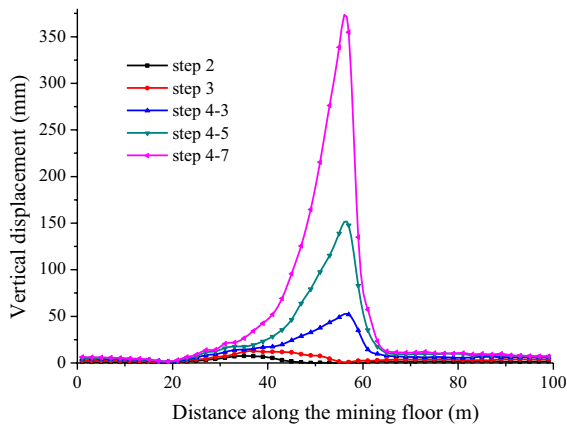
zone completely failed (Fig. 14e), and the maximum vertical displacement of the seam floor reached 354.9 mm.

Figure 16 and Fig. 17 show the computed seepage velocity field and the water flow volume in the seam floor, respectively. The arrows in the model represent the velocity vector before and after the water inrush. The longer the arrow is, the higher the flow velocity is.

It can be seen from the seepage velocity field that the fluid flow rate is basically consistent with the permeability of the rock formation. In the initial mining stage, under the influence of the high water pressure, the particle fillings in the fault were continuously washed and migrated, causing groundwater to penetrate to a certain height along the fault. Influenced by the obstruction of the aquifuge, the groundwater slowly penetrated into the aquifuge and the velocity vector was very small (Fig. 16a). The maximum water flow rate in the seam floor was 5.2 m<sup>3</sup>/min (Fig. 17). When the mining distance reached 30 m, the high-pressure water continued to impact the floor aquifuge, and the permeability increased accordingly (Fig. 16b), the water flow rate reached 9.3m<sup>3</sup>/min. When the mining-induced damage zone was connected to the fault activation zone, the seepage



**Fig. 14** The critical pathway for water inrush by the development of damage



**Fig. 15** The distribution of vertical displacement in the mine floor

velocity in the mining floor quickly increased from 21.7m<sup>3</sup>/min to 95.4m<sup>3</sup>/min (Fig. 17), resulting in a large amount of groundwater pouring into the No.866 mining face, and causing a serious water inrush accident (Fig. 16e).

The numerical results clearly illustrate the intrinsic reasons for the underground water inrush in the Zhuxianzhuang coal mine (when, where, and how). In the numerical simulation, cracks propagation, stress distribution and seepage development in the floor strata can be visually represented during the evolution of the water inrush. Some explanations for strata damage and fluid flow associated with faults are further confirmed (Babiker and Gudmundsson, 2004; Karacan et al., 2008). The RFPFA numerical software provides a more convenient and applicable method for studying the failure mechanism of rock mass and the evolution law of seepage field related to underground water inrush. When the working face advances for

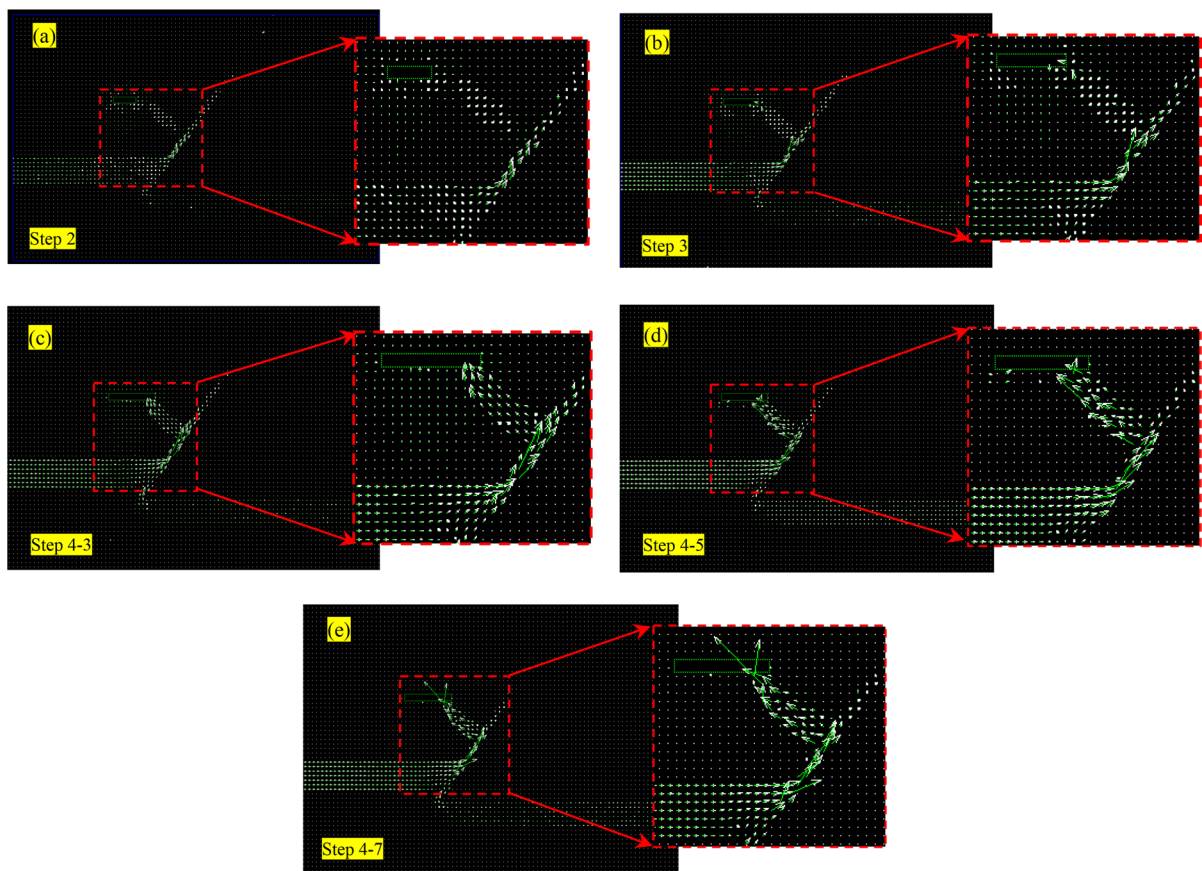


**Fig. 16** The critical pathway for water inrush by the water flow velocity

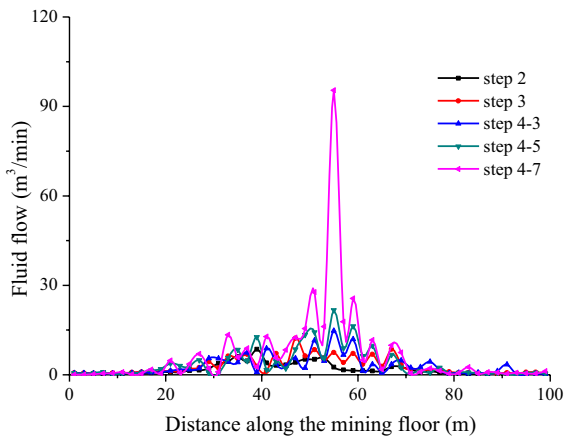


**Fig. 17** Variation of water flow volume in the mine floor

a certain distance, if there is an abnormal seepage phenomenon, preventive measures should be taken immediately to avoid water inrush hazards.

## 5 Conclusions

A similar physics experiment was carried out on the mechanism of fault seepage in the Zhuxianzhuang coal mine, and the underground water inrush mechanism caused by fault was numerically analyzed. The main conclusions were:

1. The evolution process of seepage in fault can be divided into five stages, i.e., the seepage initiation stage, the seepage development stage, the seepage mutation stage, the seepage outburst stage, and the seepage stable stage. The seepage types can be divided into pore flow, fracture flow and channel flow. During the process of pore flow to fracture flow conversion, special attention should be paid to the seepage mutation stage, it is crucial for the accurate assessment of water inrush risk. In addition, the seepage characteristics in the fault are affected not only with time but also with different geological structural conditions.
2. Mining activities and high water pressure will lead to fault activation, and the migration and loss of particle fillings in fault are the main factors for the change of seepage. With the migration and loss of particle fillings, fault porosity and permeability are increasing. Eventually, the

seepage mutation appears, leading to the formation of water inrush channels in fault.

3. When mining coal mines with faults and high-pressure aquifers (such as Zhuxianzhuang Coal Mine), according to the failure conditions of the floor strata, it can be divided into three main influenced zone, mining-induced damage zone, effective water-resisting zone and fault activation zone. Among them, the effective water-resisting zone is a key area that causes water inrush accidents, which directly determines the effective thickness of the aquifuge. The smaller the thickness is, the greater the risk of water inrush is.
4. Mining-induced fracture development and fault activation caused by high water pressure are the main factors leading to the stress distribution and mechanical strength reduction of the floor strata, and change the conventional damage mode of the floor strata, which resulting in the development of damage mainly concentrated in the aquifuge between the seam floor and fault. Once the mining-induced damage zone is completely hydraulically connected with the fault activation zone, a complete water inrush channel will be formed, and a large amount of groundwater will flood into the mining face, resulting in a water inrush disaster.

**Acknowledgements** The study is jointly supported by grants from the Key Program of National Natural Science Foundation of China (Grant No. 51534003); National Key Research and Development Program of China (Grant No. 2016YFC0801601; 2016YFC0801606; 2016YFC0801604). The authors are grateful for these supports.

**Funding** the key program of national natural science foundation of china,51534003,Jianli Cao,national key research and development program of china,2016YFC0801606,Jianli Cao

**Data Availability** Enquiries about data availability should be directed to the authors.

## Declarations

**Competing Interests** The authors have not disclosed any competing interests.

## References

- Babiker M, Gudmundsson A (2004) The effects of dykes and faults on groundwater flow in an arid land: the Red Sea Hills. *Sudan J Hydrol* 297(1):256–273
- Bieniawski ZT (1973) Engineering classification of jointed rock masses. *Civ Eng S Afr* 15:335–343
- Bieniawski ZT (1987) Determining rock mass deformability: experience from case histories. *Int J Rock Mech Min Sci Geomech Abstr* 15(5):237–247
- Cao YX, He DD, Glick DC (2001) Coal and gas outbursts in footwalls of reverse faults. *Int J Coal Geol* 48(1):47–63
- Chen JH, Li DQ (2022) Numerical simulation of fully encapsulated rock bolts with a tri-linear constitutive relation. *Tunnelling and Underground Space Technology* 120: 104265
- Chen JH, Liu P, Zhao HB, Zhang C, Zhang JW (2021a) Analytical studying the axial performance of fully encapsulated rock bolts. *Engineering Failure Analysis* 128: 105580.
- Chen JH, Zhao HB, He FL, Zhang JW, Tao KM (2021b) Studying the performance of fully encapsulated rock bolts with modified structural elements. *International Journal of Coal Science & Technology* 8:64–76
- Fang Z, Harrison JP (2002) Development of a local degradation approach to the modeling of brittle fracture in heterogeneous rocks. *Int J Rock Mech Min Sc* 39(4):443–457
- Islam MR, Shinjo R (2009) Mining-induced fault reactivation associated with the main conveyor belt roadway and safety of the Barapukuria Coal Mine in Bangladesh: Constraints from BEM simulations. *Int J Coal Geol* 79(4):115–130
- Jia MK (2012) The Study on the Deformation Process of Overlying Strata in the Deep and Thin Bedrock. *J Min Safety Eng* 29(2):168–172 ((Chinese))
- Karacan CÖ, Ulery JP, Goodman GVR (2008) A numerical evaluation on the effects of impermeable faults on degasification efficiency and methane emissions during underground coal mining. *Int J Coal Geol* 75(4):195–203
- Kong XY (2010) *Advanced Mechanics of Fluids in Porous Media*, 2nd edn. USTC Press, Hefei China
- Li H, Bai HB, Wu JJ, Wang CS, Ma ZG, Du YB, Ma K (2017) Mechanism of water inrush driven by grouting and control measures—a case study of chensilou mine, china. *Ara J Geosci* 10(21):468
- Li LC, Tang CA, Zhao XD, Cai M (2014) Block caving-induced strata movement and associated surface subsidence: a numerical study based on a demonstration model. *B Eng Geol Environ* 73(4):1165–1182
- Li LC, Tang CA, Liang ZZ (2010) Investigation on overburden strata collapse around coal face considering effect of broken expansion of rock. *Rock Soil Mech* 31(11):3537–3541
- Li LC, Yang TH, Liang ZZ, Zhu WC, Tang CA (2011) Numerical investigation of groundwater outbursts near faults in underground coal mines. *Int J Coal Geol* 85(3–4):276–288
- Liu SL, Liu WT, Shen JJ (2017) Stress evolution law and failure characteristics of mining floor rock mass above confined water. *KSCE J Civ Eng* 21(7):2665–2672
- Liu Z, Xiong C (2007) Numerical simulation study on water inrush mechanism from collapse column. *Chin J Rock Mech Eng* 26:4013–4018 ((Chinese))
- Lu Q, Li X, Li W, Liu SL (2018) Risk evaluation of bed-separation water inrush: A case study in the Yangliu coal mine. *China Mine Water Environ* 37(2):288–299
- Lu YL, Wang LG (2015) Numerical simulation of mining-induced fracture evolution and water flow in coal seam floor above a confined aquifer. *Comput Geotech* 67:157–171
- Ma D, Bai HB, Wang YM (2015) Mechanical behavior of a coal seam penetrated by a karst collapse pillar: mining-induced groundwater inrush risk. *Nat Hazards* 75(3):2137–2151
- Ma GW, Wang XJ, Ren F (2011) Numerical simulation of compressive failure of heterogeneous rock-like materials using SPH method. *Int J Rock Mech Min Sci* 48(3):353–363
- Minkoff SE, Stone CM, Bryant S, Peszynska M, Wheeler MF (2003) Coupled fluid flow and geomechanical deformation modeling. *J Petrol Sci Eng* 38(1–2):37–56
- Mohamma N, Reddish DJ, Stace LR (1997) The relation between in situ, and laboratory rock properties used in numerical modelling. *Int J Rock Mech Min Sci* 34(2):289–297
- Nicholson GA, Bieniawski ZT (1990) A nonlinear deformation modulus based on rock mass classification. *Int J Min Geo Eng* 8(3):181–202
- Niu LL, Zhu WC, Cheng Z, Guan K, Qin T (2017) Numerical simulation on excavation-induced damage of rock under quasi-static unloading and dynamic disturbance. *Environ Earth Sci* 76(17):614
- RPPA User Manual (2005) Dalian Mechsoft Co., Ltd. Dalian, China.
- Shi WH, Yang TH, Yu QL, Li Y, Liu HL (2017) A Study of Water-Inrush Mechanisms Based on Geo-Mechanical Analysis and an In-situ Groundwater Investigation in the Zhongguan Iron Mine. *China Mine Water Environ* 36(3):409–417
- Souley M, Homand F, Pepa S, Hoxha D (2001) Damage-induced permeability changes in granite: a case example at the URL in Canada. *Int J Rock Mech Min Sci* 38:297–310
- Tang CA (1997) Numerical simulation on progressive failure leading to collapse and associated seismicity. *Int J Rock Mech Min Sci* 34:249–261
- Tang CA, Tham LG, Lee PK (2002) Coupled analysis of flow, stress and damage (FSD) in rock failure. *Int J Rock Mech Min Sci* 39(4):477–489
- Wang LG, Miao XX (2006) Numerical simulation of coal floor fault activation influenced by mining. *J Chin Univ Min Technol* 16(4):385–388 ((Chinese))
- Weibull W (1951) A statistical distribution function of wide applicability. *J Appl Mech* 13(2):293–297
- Wu Q, Wang M, Wu X (2004) Investigations of groundwater bursting into coal mine seam floors from fault zones. *Int J Rock Mech Min Sci* 41(4):557–571
- Yang TH, Liu J, Zhu WC, Elsworth D, Tham LG, Tang CA (2007) A coupled flow-stress-damage model for groundwater outbursts from an underlying aquifer into mining excavations. *Int J Rock Mech Min Sci* 44(1):87–97
- Yang TH, Tham LG, Tang CA, Liang ZZ, Tsui Y (2004) Influence of heterogeneity of mechanical properties on hydraulic fracturing in permeable rocks. *Rock Mech Rock Eng* 37(4):251–275

- Yao BH, Bai HB, Zhang BY (2012) Numerical simulation on the risk of roof water inrush in Wuyang coal mine. *Int J Min Sci Technol* 22(2):237–277
- Yin SX, Zhang JC, Liu DM (2015) A study of mine water inrushes by measurements of in situ stress and rock failures. *Nat Hazards* 79(3):1961–1979
- Yuan SC, Harrison JP (2005) Development of a hydro-mechanical local degradation approach and its application to modelling fluid flow during progressive fracturing of heterogeneous rocks. *Int J Rock Mech Min Sci* 42(7):961–984
- Zhang HQ, He YN, Tang CA, Ahmad B, Han LJ (2009) Application of an improved flow-stress-damage model to the criticality assessment of water inrush in a mine: A case study. *Rock Mech Rock Eng* 42(6):911–930
- Zhang JC, Peng SP (2005) Water inrush and environmental impact of shallow seam mining. *Eng Geol* 48(8):1068–1076
- Zhang R, Jiang ZQ, Zhou HY, Yang CW, Xiao SJ (2014) Groundwater outbursts from faults above a confined aquifer in the coal mining. *Nat Hazards* 71(3):1861–1872
- Zhao HJ, Ma FS, Xu JM, Guo J (2012) In situ stress field inversion and its application in mining-induced rock mass movement. *Int J Rock Mech Min Sci* 53:120–128
- Zeng YF, Wu Q, Liu SQ, Zhai YL, Lian HL, Zhang W (2017) Evaluation of a coal seam roof water inrush: case study in the Wangjialing coal mine. *China Mine Water Environ* 37(3):1–11
- Zhu WC, Wei CH (2011) Numerical simulation on mining-induced water inrushes related to geologic structures using a damage-based hydromechanical model. *Environ Earth Sci* 62(1):43–54
- Zuo JP, Peng SP, Li YJ, Chen ZH, Xie HP (2009) Investigation of karst collapse based on 3-D seismic technique and DDA method at Xieqiao coal mine. *China Int J Coal Geol* 78(4):276–287

**Publisher's Note** Springer Nature remains neutral with regard to jurisdictional claims in published maps and institutional affiliations.